Metastable structures of solid hydrogen

G. W. Collins, W. G. Unites, E. R. Mapoles, and T. P. Bernat

Lawrence Livermore National Laboratory, Livermore, California 94551

The $J=0 \rightarrow 2$ Raman signal from solid $J=0$ D_2 or H_2 reveals the hcp structure when deposited at a rate $0.1 \leq R(\mu m/min) \leq 40$ onto MgF_2 at $T_d/T_{tp} > 0.3$, a mixture of hcp and fcc crystals at $0.2 < T_d/T_{tp} < 0.3$ and possibly a randomly stacked close-packed structure at $T_d/T_{tp} < 0.2$, where T_{tp} is the triple point temperature. Non-hcp crystals transform to hcp continuously and irreversibly with increasing T. Finally, the crystal size decreases with decreasing T_d and increasing R, from ~ 1 mm at $T_d \sim 0.8 T_{tp}$ and $R \sim 2$ $\mu m/min$ to ~ 1 μm at 0.25 T_{tp} and $R \sim 40$ $\mu m/min$.

I. INTRODUCTION

Near the triple point temperature T_{tp}, H_2 and D_2 typically form an hcp structure.[1,2] Since the interaction between hydrogen molecules is weak, the rotational quantum number is well defined in the low-pressure solid at temperatures above 0.2 T_{tp} and most of the molecules are either in the ground ($J=0$) or first exited ($J=1$) rotational state. At low enough temperature and large $J=1$ concentration, $[J=1] > 55\%$, the lattice transforms to fcc with the molecules ordered. This phase transition lowers the electric quadrupole-quadrupole energy for $J=1$ molecules by about 5 K/molecule, which is much greater than the ~ 1 mK/molecule energy difference between disordered hcp and fcc structures. In $J=0$ hydrogen, the free-energy difference between hcp and fcc is not well understood, but the equilibrium crystal structure at all temperatures and pressures below ~ 100 GPa is hcp.[3]

Rare-gas solids also form simple molecular solids with lattice potentials similar to hydrogen. However, Ne, Ar, Kr, and Xe crystallize into fcc at low pressure, while the lightest rare gas, ^{4}He, primarily forms hcp structure at low temperature and pressure, and fcc only at high temperature and pressure. The hcp structure forms in low pressure ^{4}He and possibly $J=0$ hydrogen because the dispersion interaction for the closed-shell S state orbital is comparatively small.[4]

While hcp is the equilibrium structure at low $J=1$ concentrations, nonequilibrium hydrogen structures are observed.[1] Mills, Yarnell, and Schuch sprayed D_2 into liquid helium at 4.2 K where it formed D_2 powder with fcc structure, reverting to hcp structure when heated.[5] Also, thin (~ 10 nm) films deposited below ~ 0.4 T_{tp} have shown metastable fcc structure.[6,7] Finally, thin hydrogen films grown from the vapor or liquid can take on the lattice structure of the substrate.[8] We will fill a gap in this literature by describing the temperature dependence and the crystal morphology of the metastable phases in $J=0$ H_2 and D_2. We show, (1) the metastable fcc phase is separated from hcp by a spectrum of energy barriers, (2) impurities can increase the energy barriers separating fcc and hcp, (3) the fcc phase is less stable in H_2 than in D_2, (4) the structural symmetry decreases as T_d decreases, and (5) the crystallite length scale decreases with decreasing T_d.

To determine lattice structure we detect the $J=0 \rightarrow 2$ signal of the rotational Raman spectrum. In pure $J=0$ solids this signal produces a multiplet which can be a unique signature of the crystal lattice. A triplet is unique to hcp, whereas fcc symmetry produces a doublet. The calculational procedure for determining the spectral positions and intensity ratios are outlined by Van Kranendonk in Ref. 3. Some of our observations may be similar to those of Silvera and Wijngaarden[9] and Durana and McTague[10] who observed a four-peak spectrum in rapidly pressurized hydrogen. Four peaks are expected if the Raman signal results from both hcp and fcc crystals because the high-energy shifted peak for both hcp and fcc are close together, and the low-energy shifted fcc signal is at lower energy than the other hcp lines.

In this paper we describe the lattice structure and crystal morphology of thick (>10 μm) $J=0$ H_2 and $J=0$ D_2 layers grown from the gas phase. We observe a triplet for the $J=0 \rightarrow 2$ Raman signal, and thus the hcp structure,[11] for both H_2 and D_2 deposited on MgF_2,[12] when $T_d/T_{tp} > 0.3$ where the triple point temperatures are $T_{tp}(J=0$ $H_2) = 13.8$ K and $T_{tp}(J=0$ $D_2) = 18.7$ K.[13] At $0.2 < T_d/T_{tp} < 0.3$ we resolve four narrow peaks for this Raman transition which we show is due to a mixture of hcp and fcc crystallites. When $T_d/T_{tp} < 0.2$, the signal is unresolved with two main branches, indicating a structure with less symmetry than fcc or hcp. The two- and four-peak multiplets transform continuously and irreversibly into a triplet upon increasing T through $0.5 T_{tp}$. Codepositing $<1\%$ N_2 in $J=0$ D_2 at $\sim 0.3 T_{tp}$ stabilizes more of the fcc phase as compared to pure D_2. Finally, we show that the size of H_2 or D_2 crystallites decreases with decreasing T_d and increasing R, from millimeter scale at $T_d \sim 0.8 T_{tp}$ and $R \sim 2$ $\mu m/min$ to micron scale at $T_d \sim 0.3 T_{tp}$ and $R \sim 40$ $\mu m/min$.

II. EXPERIMENTAL DETAILS

For these experiments, a copper sample cell is fitted with two opposing vertical MgF_2 coated sapphire windows, which serve as the hydrogen substrate and permit optical access. The cell is connected to the cold tip of a helium flow cryostat. Both a 30 K radiation shield and the outer vacuum jacket contain sapphire windows for optical access. A calibrated germanium resistance thermometer (GRT) is fitted on the copper sample cell and checked against T_{tp} of D_2 and H_2. At $T > 0.5 T_{tp}$, we compare the thermometer temperature with the temperature from the hydrogen vapor pressure[14] measured by a capacitance manometer. The agreement be-
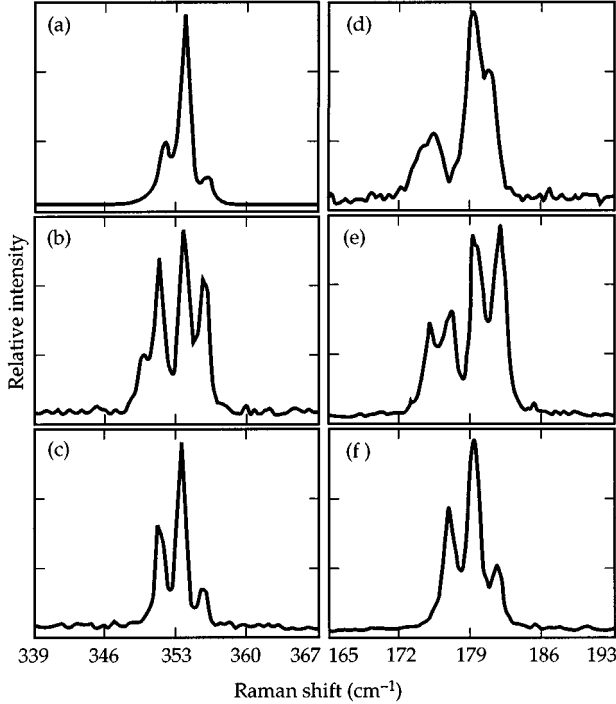
FIG. 1. $J=0$ to 2 Raman signal for (a) H_2 deposited at 5.5 K and 5 μm/min, (b) H_2 deposited at 3.5 K and 2 μm/min, (c) same sample as (b) after warming from 3.5 to 7 K, (d) D_2 deposited at 3.5 K and 0.2 μm/min, (e) D_2 deposited at 5.2 K and 0.4 μm/min, (f) same sample as (e) after warming from 5.2 to 11.4 K.

tween the vapor pressure and the GRT determines the accuracy of the temperature measurement to be better than 0.05 K.

The H_2 and D_2 gas were high-purity research grade with an isotopic purity of 99.9% and 99.8%, respectively. The samples studied contained a $J=1$ concentration less than ~1%. The rotational and isotopic concentration is determined by comparing the Raman line intensities for the $J=0\rightarrow2$ and $J=1\rightarrow3$ transitions. The hydrogen gas was cooled to ~20–30 K just before deposition. The deposition rates are determined from the layer thickness, measured by interferometry, versus time. All the samples were between 30 and 300 μm thick.

We measured the Raman shift of the 488 nm line of an Ar ion laser in backscattering geometry with a modified 1/2 meter SPEX 1870 spectrograph fitted with a liquid-nitrogen-cooled CCD having a 22.5 μm pixel width. We used F/3 optics to couple light in and out of the sample. Our spectral resolution was ~0.4 cm^{-1}. Line positions were determined from both a calibrated thorium lamp and the triplet structure of H_2 or D_2 crystallized through the triple point, with their line positions as measured by Bhatnagar, Allin, and Welsh.[16] The laser power level (~1–100 mW in ~40 μm^2) did not influence the lattice structure or visually change the layer morphology.

III. RAMAN DATA

Figure 1 shows the Raman signal for our layers. The three-peak spectrum in Fig. 1(a) is typical of H_2 and D_2 at $T_d>0.3T_{tp}$. The four-peak spectra in Figs. 1(b) and 1(e) are typical of 3.5 K$\lesssim T_d(H_2)<4$ K and 4 K$<T_d(D_2)\lesssim6$ K and
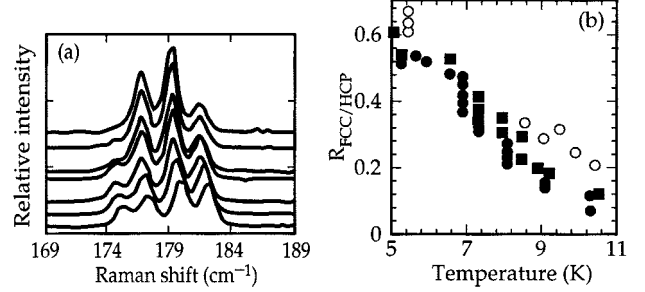

FIG. 2. Temperature and time dependence of the $J=0\rightarrow2$ Raman spectrum, upon warming solid $J=0$ D_2. (a) D_2 deposited at 5.3 K and 2.2 μm/min; From bottom to top (i) after deposition at 5.3 K, (ii) after raising the temperature to 6.9 K, (iii) after waiting at 6.9 K for 34 min, (iv) after raising the temperature to 7.4 K and waiting 8 min, (v) after 13 min at 8.1 K, (vi) after 5 min at 9.1 K, and (vii) after 2 min at 10.4 K. (b) The low-energy Raman peak divided by the average of the other three peaks ($R_{fcc/hcp}$) versus temperature from three different experiments. The dark circles show the same experiment as in (a). Dark squares show a similar experiment with $J=0$ D_2 deposited at 5.1 K and 0.4 μm/min. After deposition the sample sat at ~5.3 K for 23 h and then we began raising the temperature at about 0.5 K/20 min. Open circles show $J=0$ D_2+0.05% N_2 deposited at 5.5 K and 2 μm/min.

deposition rates between $0.1<R(\mu$m/min$)<40$. Figure 1(d) is typical for $3.5\lesssim T_d(D_2)<4$ K where it appears the peaks in Fig. 1(e) shift towards an unresolved line shape with two main branches. Figures 1(c) and 1(f) show the signals several minutes after rapidly warming H_2 and D_2, respectively. The quadruplet in Figs. 1(b) and 1(e) and the unresolved "doublet" in Fig. 1(d) transform to a triplet within minutes upon warming the sample rapidly through ~$0.5T_{tp}$. At constant temperature the Raman spectra in Fig. 1 are stable for at least two days, the maximum duration of observation.

Figure 2(a) shows the temperature dependence of the Raman spectrum of D_2. The steady decrease in the relative intensity of the first and fourth peak with increasing temperature is not reversible upon cooling. There is a slight shift in the spectrum of ~-0.45 cm^{-1} upon warming from 5 to 7 K. The high-energy peak may be shifted slightly more (~-0.70 to -0.90 cm^{-1}) than the other low-energy peaks. The quadruplet signal in H_2 also transforms to a triplet upon slowly raising T to ~5.5 K.

In Fig. 2(b) we plot the intensity ratio of the low-energy Raman peak of the quadruplet divided by the average of the other three peaks, $R_{fcc/hcp}$ vs temperature (all values, not just the steady-state value) from three different experiments. The large scatter of points at each temperature is primarily due to the complicated time dependence at constant temperature and the lowest value for $R_{fcc/hcp}$ is the steady-state value. The plot is approximately linear from 6 to 11 K. For D_2 deposited between 5.1 and 5.5 K and held at constant temperature for ~2 days there is no change in $R_{fcc/hcp}$. Thus, $R_{fcc/hcp}$ is roughly constant at constant temperature, decreases with increasing temperature, and evolves to steady state in several minutes.

The unresolved broad doublet for D_2 in Fig. 1(d) shows a different behavior. Upon increasing T from T_d~3.5 to 7 K the two overlapping lines in the right-hand branch separated slightly but the general structure still consisted of two main branches. Upon increasing T to ~10 K, the structure trans-

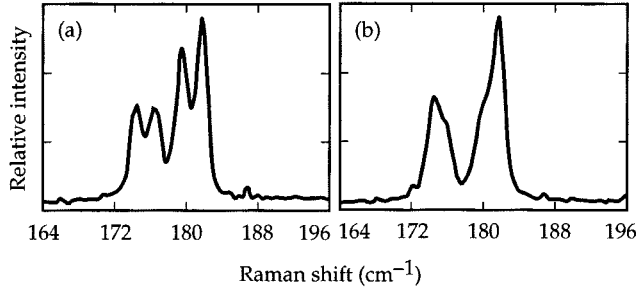FIG. 3. $J=0\rightarrow2$ Raman spectra for (a) $J=0$ $D_2+0.05\%$ N_2 deposited at 5.5 K and 2 μm/min, and (b) $J=0$ $D_2+0.5\%$ N_2 deposited at 5.5 K and 2 μm/min.

formed into a well resolved triplet similar to that shown in Fig. 1(f), within ~10 min.

Figure 3 shows the effect of codepositing N_2 with D_2. Comparing Fig. 3(a) with Fig. 1(e) shows 0.05% N_2 in D_2 affects the Raman transition only slightly, but Fig. 2(b) shows a slightly larger value of $R_{fcc/hcp}$ at all temperatures as compared to pure D_2. The first three points in Fig. 2(b) were taken 1 h apart and decreased with time at the constant temperature of 5.5 K to $R_{fcc/hcp}$~0.6. The sample warmed up slowly over the next 12 h to 8.6 K. The rest of the data were taken allowing the sample to relax for ~10 min after each temperature increase. Figure 3(b) ($D_2+0.5\%$ N_2) shows a broad unresolved signal, similar to Fig. 1(d), but with $T_d>4$ K. This broad signal was stable up to ~17 K for several minutes.[15]

IV. DISCUSSION OF RAMAN DATA

In Table I we list the theoretical and measured line positions for the Raman multiplet for both hcp and fcc crystal structures. We calculate the theoretical values from Van Kranendonk.[3] The measured values are from the present work and Bhatnagar, Allin, and Welsh.[16] The calculated values for the hcp lattice are close to the measured values. The calculated low-energy line of an fcc structure is at the same position as the low-energy line of the quadruplet spectrum in Figs. 1(b) and 1(e). The calculated high-energy line of the fcc lattice would be unresolved from the high-energy hcp line given our resolution. Because of the low-energy line position in the quadruplet spectrum and the change in intensity of the high-energy line upon warming to $T=0.5T_{tp}$, we interpret the quadruplet spectrum to be the signature of a mixed hcp and fcc lattice. The narrow-line resolved spectra

of Figs. 1(b) and 1(e) are from regions of hcp or fcc structure, possibly small hcp or fcc crystallites.

The relative $m_j=1$, 2, 0 intensity ratios for Figs. 1(a), 1(c), and 1(f) are 0.33:1:0.15, 0.55:1:0.21, and 0.64:1:0.34. The relative m_j intensities depend on crystal orientation with respect to the incident and scattered electric-field polarizations.[3,17] Assuming the incident light is collimated, a powder average of hcp crystallites yields 1:1:0.5 and a crystal with it's c axis perpendicular to the substrate yields 0:1:0. Thus, there is a preferential c-axis alignment perpendicular to the substrate. Although a preferential growth along the c axis has been observed near the triple point, it is unclear why these small crystals would grow in a preferred direction or transform from fcc to hcp in a preferred orientation.

As T_d decreases between $0.2<T_d/T_{tp}<0.3$ the intensity of the low- and high-energy peaks increases relative to the two central peaks. After deposition, as T is increased towards $0.5T_{tp}$, the low- and high-energy peaks decrease. This is expected if an fcc component occurs at $T_d/T_{tp}<0.3$ and increases with decreasing T_d. This is why we defined the ratio $R_{fcc/hcp}$ which is a relative measure of fcc to hcp structure in the sample. The irreversible decrease in $R_{fcc/hcp}$ with increasing temperature suggests the fcc component, once formed, is metastable at $T<0.5T_{tp}$. The equilibration of $R_{fcc/hcp}$ after each temperature increase suggests the fcc phase is separated from the lower energy hcp phase by many different barrier energies. Since the outside peaks of the line shape from N_2 doped D_2, shown in Fig. 3, are relatively larger than in the corresponding line shapes in pure D_2, shown in Fig. 1, we conclude that codepositing N_2 with hydrogen increases the fraction of fcc structure. Because fcc structure in D_2 persists to higher temperatures with the addition of N_2, we conclude that N_2 increases the energy barriers separating hcp and fcc structure. We have seen a similar effect when codepositing Ne in D_2, although the amount of Ne required to stabilize a spectrum similar to Fig. 3(b) is close to 50%.

At constant T_d we also see a slight increase in the fcc component with decreasing R. This implies that the fcc component may be found at $T_d/T_{tp}>0.3$ if we deposited at lower R. This effect may be due to sample heating.

Relative to their triple points, the temperature at which the mixed fcc+hcp structure is formed is lower in H_2 (~4 K) than in D_2 (~6 K). Also, the mixed phase transforms to pure hcp at a relatively lower temperature in H_2 (~5.5 K) than in D_2 (~10.5 K). Thus the FCC phase is less stable in H_2 than in D_2. If the fcc phase is metastable and separated from the hcp phase by a spectrum of energy barriers, and if tunneling is a dominant mechanism for molecular motion at these low temperatures, then H_2 would be able to cross the energy bar-

TABLE I. Calculated and measured $J=0\rightarrow2$ Raman line positions (in cm^{-1}) for H_2 and D_2 in hcp and fcc phases.

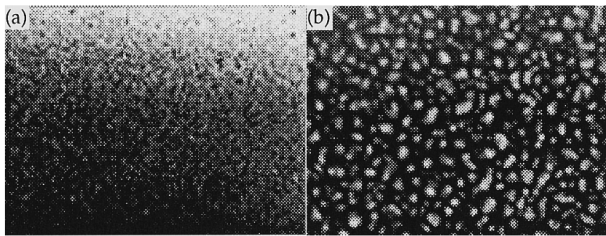|	H$_2$			D$_2$		
	Calc.	Ref. 16	Fig. 1	Calc.	Ref. 16	Fig. 1
Hcp						
$m_j=2$	354.5	353.85	354	179.6	179.4	179
$m_j=1$	352.0	351.84	352	176.5	176.8	177
$m_j=0$	357.0	355.83	356	182.7	182.0	182
Fcc						
E_1	349.6		350	173.6		175
E_2	356.9		356	182.6		182

FIG. 4. Shadowgraph images of H_2 deposited at 40 μm/min and (a) 3.6 K and (b) 7.0 K. The horizontal field of view is 1.7 mm.

FIG. 5. Average crystallite diameter versus deposition temperature for H_2 deposited at 0.2 μm/min (dark squares), 2 μm/min (dark circles), and 40 μm/min (dark triangles).

riers to reach the lower energy hcp phase more rapidly than D_2. Although tunneling diffusion has been observed for hydrogen atoms in solid hydrogen,[18] tunneling of molecules in solid hydrogen has not been clearly observed.[19]

The unresolved line shape of Fig. 1(d) is significantly different than the other narrow line spectra in Fig. 1. This broad line shape indicates that the lattice structure of samples deposited at $T_d < 0.2 T_{tp}$ have less symmetry than pure hcp or fcc.[13] The broad line shape may result from a randomly stacked close-packed lattice, but probably not an amorphous structure, which would give rise to a single broad line similar to that of the liquid phase.

V. CRYSTAL MORPHOLOGY

Figures 4(a) and 4(b) show shadowgraph images of H_2 deposited at $R = 40$ μm/min and $T_d = 3.6$ and 7.0 K. These and similar experiments qualitatively show the average crystal size decreases rapidly with decreasing temperature and increasing deposition rate between $3.6 < T_d < 11$ K and $0.1 < R(\mu\text{m/min}) < 40$. Figure 5 shows the change in the average crystal diameter versus temperature at different deposition rates. The smallest crystal diameter is at the limit of our optical resolution ~ 3 μm and is thus a very rough estimate.[20]

Since the deposition temperatures used here are below the roughening transition temperatures for the low-energy crystal facets,[21] the lowest free-energy configuration is in the form of faceted crystallites. The appearance of smooth rounded crystallites as in Fig. 4(b) implies the crystal morphology is nonequilibrium and is determined by kinetics. To qualitatively understand the dependence of crystal size on temperature and deposition rate, we assume the temperature controls the rate at which molecules relax from a high-energy to low-energy configuration. We expect the lowest energy site to be that with the maximum number of neighboring bonds such as a step edge of a crystal. As the temperature decreases and/or the deposition rate increases the probability of finding a low-energy site before the next layer of material covers the substrate decreases.
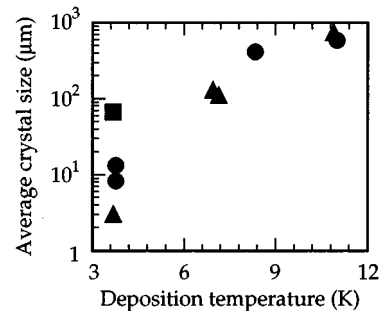
VI. CONCLUSION

In summary, using Raman spectroscopy we find $J=0$ D_2 or $J=0$ H_2 form fcc structure when deposited at $0.2 < T_d/T_{tp} < 0.3$. The fcc phase is less stable in H_2 than D_2. This fcc component transforms continuously and irreversibly to hcp upon increasing the temperature through $0.5 T_{tp}$, suggesting the fcc phase is separated from the lower energy hcp phase by a spectrum of barrier energies. As T_d decreases below $\sim 0.2 T_{tp}$ the lattice structure has less symmetry than fcc or hcp and possibly resembles a randomly stacked close-packed phase. Finally, the crystallite size decreases with decreasing T_d from millimeter scale at a few degrees below T_{tp} to micron scale at $\sim 0.3 T_{tp}$. Thus, there is decreasing structural symmetry and crystallite length scale with decreasing T_d.

The metastable hydrogen structure described here may elucidate several recent experiments. D atoms in solid deuterium deposited from the gas phase at ~ 3 K have a significantly different activation energy than expected for the equilibrium hcp structure.[18,22] Also, surface state electron mobility[23] shows an increased conductivity after annealing vapor-deposited films. These observations can at least qualitatively be explained by the metastable structures described here and those that may be found at lower deposition temperatures.

[1] Isaac F. Silvera, Rev. Mod. Phys. **52**, 393 (1980).

[2] P. C. Souers, *Hydrogen Properties for Fusion Energy* (University of California, Berkeley, 1986), Chap. 6.

[3] Jan Van Kranendonk, *Solid Hydrogen* (Plenum, New York, 1983), p. 226.

[4] K. F. Niebles and J. A. Venables, in *Rare Gas Solids*, edited by M. L. Klein and J. A. Venables (Academic, New York, 1976), Vol. 1, Chap. 9.

[5] R. L. Mills, J. L. Yarnell, and A. F. Schuch, in *Proceedings of the Low Temperature Physics Conference 13, Boulder* (Plenum,

New York, 1973), Vol. II, p. 202.

[6] O. Bostanjoglo and R. Kleinschmidt, J. Chem. Phys. **46**, 2004 (1967).

[7] A. E. Curzon and A. J. Mascall, Brit. J. Appl. Phys. **16**, 1301 (1965).

[8] C. S. Barrett, L. Meyer, and J. Wasserman, J. Chem. Phys. **45**, 834 (1966).

[9] I. F. Silvera and R. J. Wijngaarden, Phys. Rev. Lett. **47**, 39 (1981). R. J. Wijngaarden, Ph.D. thesis, Harvard University, 1982.

[10] S. C. Durana and J. P. McTague, Phys. Rev. Lett. **31**, 990 (1973).

[11] The MgF_2 was an amorphous or nanocrystalline thin film, vapor deposited onto a sapphire window which was cleaved normal to the c axis.

[12] Reference 2, p. 80.

[13] Reference 3, Chap. 4.

[14] Reference 2, p. 49.

[15] After melting the D_2+0.5% N_2 sample, N_2 plated on the windows; then when a thin film of D_2 was frozen near the triple point onto the N_2, there were only two narrow peaks in the $J=0\rightarrow2$ Raman spectrum at 175 and 182 cm^{-1}, indicating fcc structure.

[16] S. S. Bhatnagar, E. J. Allin, and H. L. Welsh, Can. J. Phys. **40**, 9 (1962).

[17] J. P. McTague, I. F. Silvera, and W. N. Hardy, *Proceedings of the 7th AIRAPT Conference on Light Scattering in Solids, Paris, France, 1971* (Flammarion Sciences, Paris, 1971), p. 456.

[18] G. W. Collins *et al.*, Phys. Rev. B **45**, 549 (1992); A. S. Iskovskikh *et al.*, Sov. Phys. JETP **64**, 1085 (1986).

[19] J. R. Gaines, Phys. Rev. B **52**, 7243 (1995).

[20] Crystals left at constant temperature, even near 3.5 K, appeared to increase with time, although we did not study this phenomena in detail. The crystal size for $T>0.7T_{tp}$ also depends on layer thickness. For the data in Fig. 5, the layers are about 50 μm thick.

[21] G. W. Collins *et al.* (unpublished).

[22] A. V. Ivliev *et al.*, JETP Lett. **38**, 379 (1983); E. B. Gordon *et al.*, *ibid.* **37**, 282 (1983).

[23] M. A. Paalanen and Y. Iye, Surf. Sci. **170**, 80 (1986); K. Kono, U. Albrecht, and P. Leiderer, J. Low Temp. Phys. **82**, 279 (1991).